



HAL
open science

On-Chip Fabrication of Colloidal Suprastructures by Assembly and Supramolecular Interlinking of Microgels

Se-hyeong Jung, Fabian Meyer, Sven Hörnig, Michelle Bund, Bernhard Häbel, Luis Paulo Busca Guerzoni, Laura de Laporte, Ghazi Ben Messaoud, Silvia P Centeno, Andrij Pich

► **To cite this version:**

Se-hyeong Jung, Fabian Meyer, Sven Hörnig, Michelle Bund, Bernhard Häbel, et al.. On-Chip Fabrication of Colloidal Suprastructures by Assembly and Supramolecular Interlinking of Microgels. *Small*, 2023, 10.1002/sml.202303444 . hal-04330439

HAL Id: hal-04330439

<https://hal.inrae.fr/hal-04330439>

Submitted on 8 Dec 2023

HAL is a multi-disciplinary open access archive for the deposit and dissemination of scientific research documents, whether they are published or not. The documents may come from teaching and research institutions in France or abroad, or from public or private research centers.

L'archive ouverte pluridisciplinaire **HAL**, est destinée au dépôt et à la diffusion de documents scientifiques de niveau recherche, publiés ou non, émanant des établissements d'enseignement et de recherche français ou étrangers, des laboratoires publics ou privés.

On-Chip Fabrication of Colloidal Suprastructures by Assembly and Supramolecular Interlinking of Microgels

*Se-Hyeong Jung, Fabian Meyer, Sven Hörnig, Michelle Bund, Bernhard Häßel, Luis Paulo Busca Guerzoni, Laura De Laporte, Ghazi Ben Messaoud, Silvia P. Centeno, and Andrij Pich**


In this report, a versatile method is demonstrated to create colloidal suprastructures by assembly and supramolecular interlinking of microgels using droplet-based microfluidics. The behavior of the microgels is systematically investigated to evaluate the influence of their concentration on their distribution between the continuous, the droplet phase, and the interface. At low concentrations, microgels are mainly localized at the water–oil interface whereas an excess of microgels results, following the complete coverage of the water–oil interface, in their distribution in the continuous phase. To stabilize the colloidal suprastructure, on-chip gelation is introduced by adding natural polyphenol tannic acid (TA) in the water phase. TA forms interparticle linking between the poly(*N*-vinylcaprolactam) (PVCL) microgels by supramolecular interactions. The combination of supramolecular interlinking with the variation of the microgel concentration in microfluidic droplets enables on-chip fabrication of defined colloidal suprastructures with morphologies ranging from colloidosomes to colloidal supraballs. The obtained supracolloidal structures exhibit a pH-responsive behavior with a disintegration at alkaline conditions within a scale of seconds. The destabilization process results from the deprotonation of phenolic groups and destruction of hydrogen bonds with PVCL chains at higher pH.

1. Introduction

Emulsions stabilized via particles adsorption at fluid–fluid interfaces and resulting in a decrease of the interfacial energy,^[1,2] were first reported by Ramsden and Pickering.^[3,4] The so-called Pickering emulsions have been employed to fabricate microcapsules by the accumulation of particles at the fluid–fluid interface and their assembly using different strategies such as polymerization,^[5,6] sintering,^[7] annealing,^[8] chemical interlinking,^[9,10] and physical interlinking like electrostatic and van der Waals interactions.^[11,12] These hollow capsules with a shell composed of densely packed colloidal particles are called colloidosomes by analogy with liposomes.^[11–15] Colloidosomes are generally spherical and have tunable characteristics such as size, wall thickness, rigidity, porosity. Their tunable properties make them attractive candidates for encapsulation and smart coatings applications.^[11,12]

S.-H. Jung^[+], F. Meyer, S. Hörnig, M. Bund, A. Pich
Functional and Interactive Polymers
Institute of Technical and Macromolecular Chemistry
Worringerweg 2, 52074 Aachen, Germany
E-mail: pich@dwi.rwth-aachen.de

S.-H. Jung^[+], F. Meyer, S. Hörnig, M. Bund, B. Häßel, L. P. B. Guerzoni,
L. De Laporte, G. Ben Messaoud^[++], S. P. Centeno, A. Pich
DWI-Leibniz Institute for Interactive Materials e.V.
Forckenbeckstr. 50, 52074 Aachen, Germany

 The ORCID identification number(s) for the author(s) of this article can be found under <https://doi.org/10.1002/smll.202303444>

[+] Present address: Laboratory for Soft Materials and Interfaces, Department of Materials, ETH Zurich, Zurich 8093, Switzerland

[++] Present address: STLO, INRAE, Institut Agro, 65 rue de Saint-Brieuc, Rennes 35042, France

© 2023 The Authors. Small published by Wiley-VCH GmbH. This is an open access article under the terms of the Creative Commons Attribution-NonCommercial License, which permits use, distribution and reproduction in any medium, provided the original work is properly cited and is not used for commercial purposes.

DOI: 10.1002/smll.202303444

B. Häßel, L. De Laporte
Advanced Materials for Biomedicine
Institute of Technical and Macromolecular Chemistry
RWTH Aachen University
Worringerweg 2, 52074 Aachen, Germany

L. De Laporte
Institute for Applied Medical Engineering
University Hospital RWTH Aachen
Pauwelsstr. 30, 52074 Aachen, Germany

A. Pich
Aachen Maastricht Institute for Biobased Materials (AMIBM)
Maastricht University
Brightlands Chemelot Campus
Urmonderbaan 22, RD Geleen 6167, The Netherlands

Most colloidosomes reported in the early years are nonresponsive with built-in pore sizes that cannot be changed. This limitation results from their construction using hard nanoparticles. To overcome this poor performance, constraint microgels have been employed to prepare stimulus-responsive colloidosomes.^[16–18] Microgels are colloidal polymer networks with tunable chemical composition and controlled size. This enables control over water content, mechanical properties, and biocompatibility, opening attractive possibilities for different bio-related applications. Moreover, the interior of individual microgel networks allows for the encapsulation of bio-related compounds, such as drugs, proteins, DNA, and provides a large surface area for multivalent bioconjugation.^[19–22] The first example of the utilization of responsive microgels to prepare sensitive colloidosomes was reported by Lawrence et al.^[23] They demonstrated a method to fabricate temperature-sensitive capsules based on poly(*N*-isopropylacrylamide-*co*-acrylic acid) (PNIPAM) microgels in a water-in-oil inverse emulsion. The stabilization of the microgels inside water droplets was achieved by adding poly(butadiene-*block-N*-methyl 4-vinyl pyridinium diiodide) based on ionic bonds. They could show the thermoresponsiveness of synthesized microgel-based colloidosomes, which can be applied for delivery systems. In our group, different methods for synthesizing microgel-based colloidosomes were also developed.^[24,25] Berger et al. reported a method to prepare multisensitive microgel-based colloidosomes using poly(*N*-vinylcaprolactam) (PVCL) microgels and bio-based and degradable polymer poly(4-hydroxybutyrate-*co*-4-hydroxyvalerate) (PHBV) as interlinking agent in water/chloroform.^[24] Agrawal et al. reported another method to design hybrid capsules using PVCL-based microgels and silica precursor hyperbranched polyethoxysiloxane (PEOS) in water/toluene.^[25] In both works mentioned above, the capsule size was varied by changing the polymer concentration the microgel amount during the interlinking process synthesis. Additionally, they showed the thermoresponsiveness of the designed capsules. However, uniform size distribution of the colloidosomes remains as a limitation since the control of the droplets sizes before interlinking could not be controlled precisely.

The average size and size distribution of the synthesized colloidosomes are strongly dependent on the polydispersity of the emulsion droplets during the synthesis process. They are crucial properties of colloidosomes, since they determine the amount of encapsulated material and its release kinetics. Unfortunately, the synthesis methods presented above do not show the possibility of controlling the size distribution. To fabricate microgel-based colloidosomes that each encapsulates and releases identical amounts of materials, a droplet-based microfluidic technique was recently introduced.^[26] It allows to emulsify precursor suspension as templates with a narrow size distribution. Droplets are formed in simple microfluidic devices due to the balance of interfacial tension between two immiscible fluids and the shear exerted by the continuous flow on the dispersed flow.^[27] For a selected system of two immiscible phases, finely tuning the shear rate can result in droplets with uniform sizes.^[28–31] To this regard, Shah et al. designed monodisperse stimuli-responsive microgel-based colloidosomes based on a droplet-based microfluidics.^[26] They interlinked amine-functionalized PNIPAM microgels using glutaraldehyde at the water/silicon oil interface. A reversible size-change behavior over and under volume phase transition

temperature (VPTT) similar to that of their constituent microgels was successfully demonstrated. Zhang et al. prepared microcapsules (colloidosomes with hard spheres) by combining the advantages of droplet-based microfluidic platform and supramolecular host–guest chemistry. They used cucurbit[8]uril (CB[8]) to bind naphthol-modified gold nanoparticles and methyl viologen (MV²⁺) containing copolymer based on host–guest complexes.^[32] Efficient loading of fluorescein isothiocyanate-dextran (FITC-Dex) on microfluidic-chip was demonstrated. Stimuli-triggered degradation of the capsules by reduction of the MV²⁺ moiety, leading to disassembly of host–guest complexes, could clearly show the release of loaded FITC-dextran. A few years later, the same group reported a method to fabricate supramolecular colloidosomes using methyl viologen-functionalized polystyrene, polymer with naphthol unites and CB[8] based on the same supramolecular interaction.^[33] Colloidosomes were employed as carriers for encapsulation of FITC-dextran and demonstrated both a thermo- and photoresponsive release of encapsulated FITC-dextran. Ideally, a performant drug carrier would allow for an immediate release of the encapsulated molecules at the target site. The latter could be achieved by triggering the disassembly of colloidosomes supramolecular interlinks.

Tuning the shape of colloidosomes and capsules themselves toward nonspherical geometry could lead to additional attractive features like catalytic, optical, electrical, and magnetic properties.^[34] For instance, the distinctive shapes could potentially dictate their interactions with cells, leading to their potential biomedical applications.^[34] Moreover, nonspherical particles enable to pack more densely than spherical ones.^[35–37] They are beneficial for controlling suspension rheology^[38,39] and for engineering colloidal composites.^[40] However, synthesizing uniformly distributed nonspherical colloidal colloidosomes is challenging because surface tension favors spherical shapes over all length scales. Lee and Weitz reported a fabrication method of nonspherical colloidosomes using multiple compartments by a microfluidics double-emulsion technique.^[37] The morphology of the precursor droplets (double emulsions) was precisely controlled by using a glass capillary microfluidic device. Furthermore, they generated more complex structures, such as asymmetric colloidosomes, where the inner and outer surfaces of the shell are composed of different nanoparticles. This method leads to an interesting library of the colloidosomes shapes, however, the generation of a double emulsion and control over the evaporation of the fluids to modulate the shape is time-consuming. Therefore, developing a straightforward and fast approach for shape-modulation of colloidosomes remains challenging.

In our previous study,^[41] we showed the potential of an on-chip gelation method using microfluidics to produce elongated supramacromolecular microgels varying the pH in flow. In this report, we demonstrate a versatile on-chip microfluidic fabrication approach for synthesizing asymmetric, pH-sensitive microgel-based colloidosomes and colloidal suprastructures. The synthesis is achieved by combining the advantages of self-assembly of the microgels at the liquid–liquid interface, followed by the formation of supramolecular interparticle interlinks between the microgels stabilizing the nonspherical shape of the colloidosomes. Using the microgels as building blocks allows for finetuning of the shapes and internal structures of the developed colloidal assemblies by varying the production parameters.

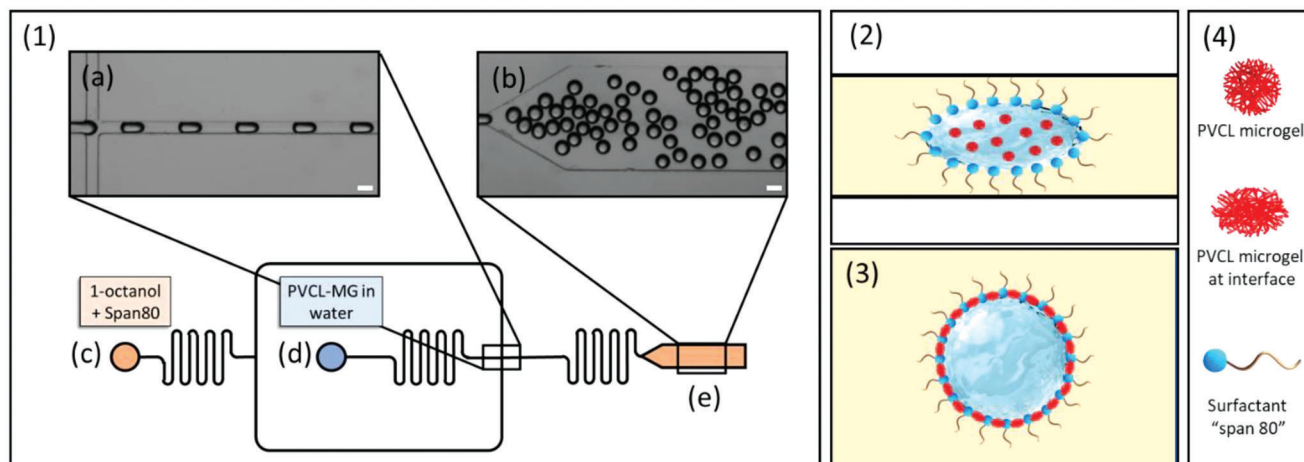
2. Results and Discussion

The aim of the present work is to synthesize pH-responsive supramolecular colloidal suprastructures, based on the PVCL-microgels and the tannic acid (TA), with different shapes and internal structures. To achieve this goal, formation of water-in-oil emulsions with different microgel concentrations had to be proceeded to examine the concentration-dependent behavior of the microgels at the interfaces. Any emulsification technique can be employed to form droplets with the aqueous microgel suspension in oil. However, since our colloidal suprastructures are developed using emulsified droplets as templates, their polydispersity is set by the distribution of droplet size. Therefore, droplet-based microfluidic technique, that can generate monodispersed population of droplets is implemented here. Next, the synthesis of the suprastructures using on-chip gelation on PDMS microfluidic chip has followed. The main challenge of this work is to control the interlinking between microgels in water droplets on microfluidic chip by varying pH while the droplets flow on a channel, so that microgels are entrapped and not dispersed in the oil phase. To show the potential in applications of the soft suprastructures, forming colloidosomes made of two different composite (microgels) is demonstrated. The assembly of different microgels into suprastructures might offer the possibility to fabricate complex larger-scale functional materials and opens up fascinating chances to fabricate multicompartiment structures with tunable functionalities.

2.1. Distribution of Microgels in Emulsion Droplets

The suitable choice of microgels is essential to obtain self-assembly behavior at the interfaces and to interlock them afterward for stable colloidosomes and supraballs. PVCL microgels are an excellent candidate due to several advantages of the polymer building blocks: 1) they show high resistance against hydrolysis and low toxicity, therefore, they are expected to be highly biocompatible,^[42] which might be crucial when it comes to bioapplications, 2) the PVCL microgels were already successfully used for formation of colloidosomes in previous research in our group,^[24,25] indicating the essential adsorption property of the microgels at the interfaces, 3) the interactions between the PVCL and the TA, which will act as supramolecular binders to interlink microgels at the surfaces to form stable suprastructures in this work have been extensively studied in the previous literature.^[41,43] The PVCL microgels with narrow size distribution are synthesized using free-radical precipitation polymerization.^[44] Additionally, a small amount of a fluorescent Rhodamine B-based comonomer (methacryloxyethyl thiocarbonyl Rhodamine B) is incorporated into the microgels.^[26,45] The synthesized microgels show an average hydrodynamic radius of 92 nm with PDI 0.16, which indicates a narrow size distribution (Figure S1 and Table S1, Supporting Information).^[46,47] Since the microgels are based on thermoresponsive polymers: PVCL, DLS measurements at different temperatures are conducted (between 16 and 50 °C).^[48,49] The experimental data suggests that the VPTT is \approx 23–25 °C (Figure S2, Supporting Information). All the microfluidic experiments were conducted at 20 °C, resulting in microgels in a swollen state in water. To investigate the self-assembly capability of the PVCL microgel at

the liquid–liquid interface, an aqueous microgels solution is dispersed in 1-octanol on the microfluidic device (**Scheme 1 (1)**). Unlike other works showing efficient emulsion stabilization by microgels in bulk systems,^[50–52] a small amount of surfactant is needed in the oil phase, which migrates to the oil–water interface and stabilizes droplets in flow systems using microfluidic chips. Therefore, 2 vol% of span 80 is dissolved as surfactant in the 1-octanol, which is used as continuous phase. Once the droplets are formed, microgels adsorb at interfaces.^[18,26,53] The image (a) shows the formation of water-in-oil emulsions at cross-junction and (b) indicates that the uniformly dispersed population of the water droplets flows on the outlet. 1-octanol containing 2 vol% of span 80 is injected into the inlet (c) as a continuous phase, while the aqueous solution containing microgels is inserted into the inlet (d) as a dispersed phase. The water droplets on the outlet (e) flow to a vial and are collected. The images of microdroplets at the outlet with two different flow rates (50 and 150 $\mu\text{L h}^{-1}$) of the water stream at varying microgel concentrations are shown in Figure S3 of the Supporting Information. Interestingly, droplets formed with low concentrations of microgels (0.5 and 1.0 mg mL^{-1}) at both flow rates start to coalesce directly on outlets after leaving the channel. From the microgel concentration of 2.5 to 20 mg mL^{-1} , no coalescence effects are observed with both flow rates, and all droplets are stable. Scheme 1 (2,3) indicates the expected structure of the emulsions with the microgels on the microfluidic device. The hypothesis is that the water droplets are formed at the cross-junction (a) and are stabilized by the surfactant molecules. Therefore, initially, microgels form colloidal dispersion within aqueous droplets (2). Afterward, the microgels adsorb at the interface and a hollow structure might emerge with low concentrations of the microgels (3). On the other hand, the full structure of droplets might be visible with higher microgel concentrations since the rest of the microgels might stay inside the droplets. To examine the location of the microgels labeled with Rhodamine B at the interfaces, confocal laser scanning microscopy (CLSM) is performed directly after the formation of the droplets (**Figure 1 (1)**). The fluorescence images (1) show emulsions formed with a flow rate of water phase 50 $\mu\text{L h}^{-1}$ while the images (Figure S4a, Supporting Information) are prepared with that of 150 $\mu\text{L h}^{-1}$. In both cases, different concentrations of the microgels are evaluated. In all samples, the red channel (from Rhodamine B fluorescence emission) is visible at the interfaces and with a greater fluorescence intensity than the core, meaning that microgels preferably adsorb and accumulate at the liquid–liquid interfaces. At low microgels concentration (0.5–1.0 mg mL^{-1}), the droplets are not stable and merge, forming larger droplets 100–600 μm , while that with higher microgel concentrations (2.5–20 mg mL^{-1}) are stable with the both flow rates. The stable droplets exhibit a uniform size distribution and comparable size, independently of the flow rate, with an average diameter of 96 and 103 μm for water flow rates of 50 $\mu\text{L h}^{-1}$ (Figure 1 (2)) and 150 $\mu\text{L h}^{-1}$ (Figure S4b, Supporting Information). Furthermore, once microgels cover droplets, they preferably disperse in octanol with increasing microgel concentrations and do not disperse inside the droplets, which contradict our expectation. Previous studies from other groups showed that the relatively polar oil octanol has greater interaction with PNIPAM-based microgels, that have similar characteristic to PVCL microgels, compared to other apolar hydrocarbon oils.^[54,55] Even



Scheme 1. 1) Schematic of the droplet generation on PDMS microfluidic device. Images show the droplet formation at cross-junction (a) and outlet (b). 1-Octanol containing 2 vol% of the surfactant “Span 80” is injected as a continuous phase (oil phase) into (c). The microgels in water are injected as dispersed phase (water phase) into (d). At the outlet (e), microdroplets flow to a collecting vial. The width of microfluidic channel is 80 μm . Graphical depiction of a water droplet on the PDMS device after first cross-junction (2) and at outlet (3) is described. (4) indicates graphical images used for the depictions. Videos for the droplet generation are available in Video S1 of the Supporting Information. The scale bars represent 100 μm .

though there are small amount of additional surfactant in the system (2 vol% of span 80) and this is not a bulk system where water, oil and microgels are stirred, this behavior: that microgels disperse greater in outer octanol phase and stabilize emulsions, agrees with empirical rules that the outer, continuous phase of an emulsion usually is the phase in which the stabilizer (microgels in this case) is more soluble (Bancroft rule) or preferentially dispersed (Finkle rule).^[45,56,57] To understand those phenomena, more focused study using the PVCL microgels with different concentrations via droplet-based microfluidic in presence of the surfactant should be conducted in the future. Another interesting result is that the sizes of droplets with higher amount of microgels show similar sizes independent on their microgel concentrations. This indicates that the microgels do not play a central role in the early stages of the emulsion formation dynamics (at the first cross-junction) as surfactants do, but in the stability of the droplets since they might adsorb at the surface after the for-

mation of the droplets. The similar phenomenon has been reported by Priest et al. where they studied the formation and stability of droplets in the presence of nanoparticles in a microfluidic device.^[58] Nevertheless, it has been clearly seen that PVCL microgels adsorbed at the water–octanol interface, which could be used to synthesize stable colloidosomes and suprastructures by interlinking them.

2.2. Fabrication of Colloidal Suprastructures

To fabricate stable colloidal structures, interlinking microgels inside water droplets as well as at the interfaces by noncovalent bonds was conducted. The microgel concentration range used was the same as from the previous emulsion study. Here, we utilized on-chip gelation with an additional cross-junction to introduce an acid moiety with a second oil phase to entrap microgels

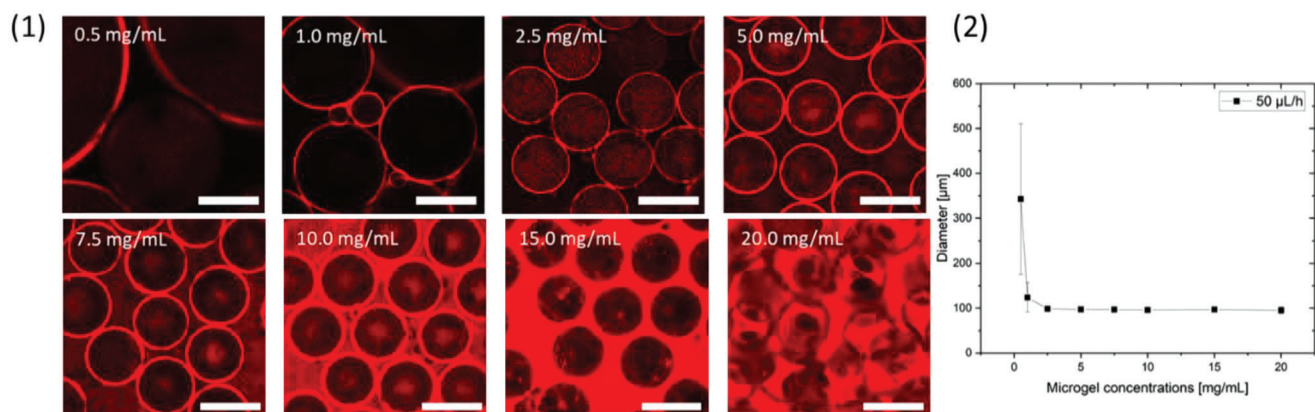
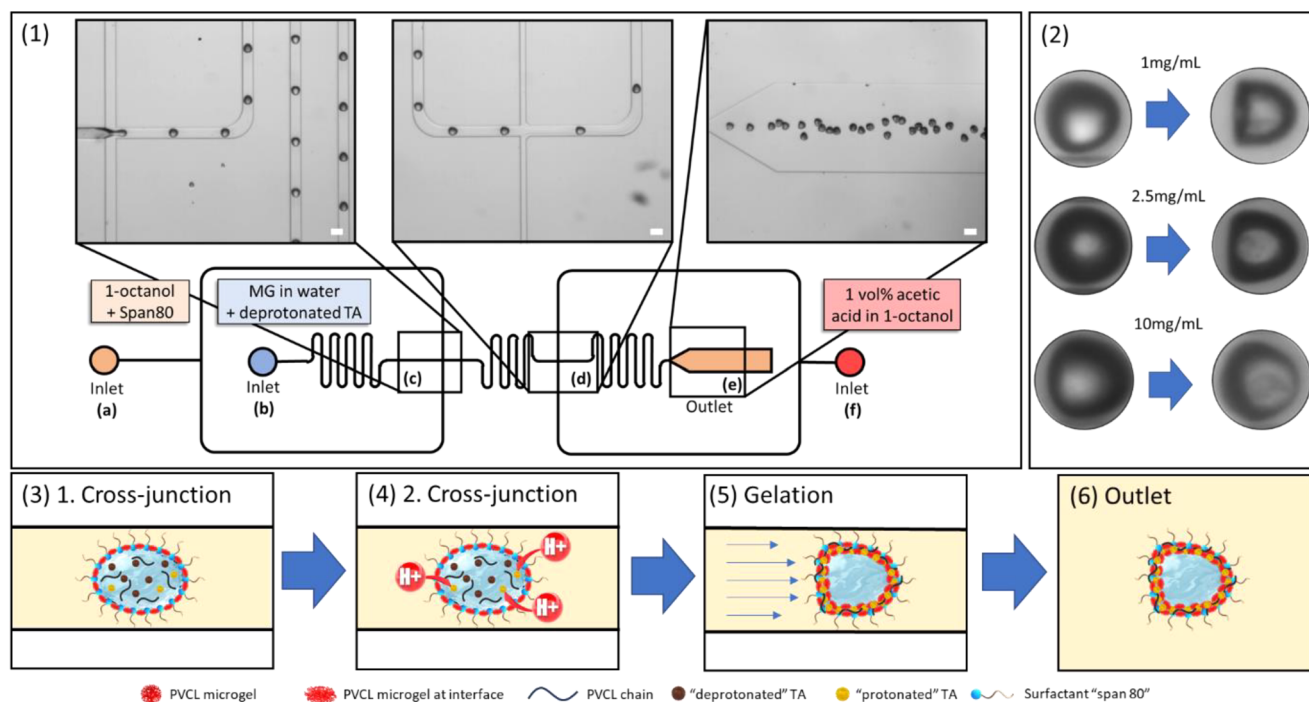


Figure 1. 1) CLSM images of water-in-oil emulsions with different microgel concentrations with the flow rates, dispersed phase: 50 $\mu\text{L h}^{-1}$, continuous phase: 400 $\mu\text{L h}^{-1}$ ($\times 63$ objective). The graph (2) indicates the diameters of the droplets. Sizes of 10 random droplets were measured from Figure S5 ($\times 10$ objective), and error bars denote standard deviations. The scale bars indicate 100 μm .



Scheme 2. 1) Schematic of the droplet generation and pH-triggered gelation on a PDMS microfluidic device. 1-octanol containing 2 vol% of the surfactant: span 80 is injected as a first continuous phase (oil phase) into the inlet (a). The polymers and deprotonated TA in water are injected as a dispersed phase (water phase) into the inlet (b). The dispersed phase is squeezed by the first continuous phase at cross-junction (c) and the image shows the generation of uniform size population of the water droplets. At the second cross-junction (d), a second continuous phase, which is injected from inlet (f), provides acidic acid to start the gelation. On outlet (e), formed colloidosomes flow to a collecting vial. The width of microfluidic channel is 80 μm and all optical images show the microfluidic fabrication process of colloidosomes on the PDMS device. The represented reaction is with 2.5 mg mL^{-1} of the microgel concentration and 3 mg mL^{-1} of the PVCL chain. The video for the synthesis is available in Video S2(1) and (2) of the Supporting Information. The scale bars represent 100 μm . 2) Optical images of gelation process at the start of the gelation (directly after second cross-junction) and at the end of the gelation on serpentine path (before outlet). 3–6) Illustrations of droplet formation and the gelation process on the microfluidic device. 3) A microwater droplet is stabilized by span 80 in octanol which is formed at the first cross-junction. 4) The PVCL microgels adsorb at the surface and protons diffuse inside the water droplets and protonate tannic acid. 5) The protonated tannic acid forms hydrogen bonds with the microgels at the surfaces and stabilizes them. The morphology is deformed by the flow on the microfluidic device. 6) The formed colloidosomes keep the structure and comes to outlet, which is connected to a vial.

inside microdroplets. This microfluidic device has already been successfully implemented to tune the shape of PVCL and TA microgels in our previous study.^[41] Scheme 2 shows the schematic illustration of an on-chip gelation using droplet-based microfluidic with a PDMS device using 2.5 mg mL^{-1} of the PVCL microgels to fabricate colloidosomes. The pH of the aqueous solution containing the PVCL microgels, the PVCL linear chains, and the TA was adjusted to 10.8–11.0 by adding NaOH (sodium hydroxide) to deprotonate TA and suppress the gelation process. The deprotonation of phenolic groups in the TA structure is essential to prevent the undesirable formation of hydrogen bonds with the carbonyl groups of the PVCL before generating droplets at the first cross-junction and to avoid clogging issues. Furthermore, these noncovalent interactions (H-bonds) might also disturb microgels to self-assemble and adsorb at the surfaces after the generation of droplets. However, alkaline conditions can alter the structures of TA due to the oxidation of phenolic groups^[59] quickly which was discussed extensively in our previous report.^[41]

In order to prevent this oxidation process, the preparation of the precursor solution is conducted under argon atmosphere and the solution is transferred directly into airtight glass syringes. Also, the addition of the small amount of the PVCL linear poly-

mers is essential to form the stable and nonspherical colloidosomes and gels. Regarding the stability of the synthesized colloidosomes and gels with and without the PVCL polymers, the details are discussed below. For the droplet formation, an aqueous precursor solution and octanol containing surfactant are injected into two separate inlets on a PDMS chip (Scheme 2 (1) (a) for the continuous phase and (b) for the dispersed phase). These two immiscible fluids meet at the first cross-junction (c) and water-in-oil droplets are generated. This process can be observed in the microscopy image (inset) showing the generation of a uniform population of micro droplets. When they flow to the second cross-junction (d), an additional octanol phase (which is injected to inlet (f) and contains 1 vol% of acetic acid emerged) provides protons to start the interlinking process between the microgels, the PVCL chains, and the TA at the interfaces. The freshly synthesized colloidosomes flow to (e) which is connected to a collecting vial. Scheme 2 (3)–(6) depicts the fabrication process on microfluidic devices while (2) displays optical images showing deformation of the microdroplets on-chip gelation that are happening between ((4) direct after addition of the second oil phase and (5) at the end of the serpentine). Microdroplets in octanol containing the PVCL microgels, the PVCL linear polymers and the

deprotonated TA are formed at the first cross-junction stabilized by span 80 (3). After the droplets leave the first cross-junction (c), the microgels adsorb at the interfaces between water and octanol and might stabilize further the water droplets. At the second cross-junction, additional octanol phase containing 1 vol% of acetic acid provides protons to activate TA (4). The protonated TA and the PVCL linear polymers build supramolecular interactions (mostly hydrogen bonds), which can act as binder between the microgels at the surfaces (5) forming stable supramolecular colloidosomes. In this step, the structure of the colloidosome is deformed due to the hydrodynamic stress from the flow. The deformed particle could be visible on the outlet (e), and they are stable after leaving the channel (6). All the deformation process of the microdroplets and particles with on-chip gelation could be seen in the optical images (2). According to the literatures, hydrodynamic forces and boundary confinement lead to a large deformation of capsules, which can take either a parachute or a slug shape.^[60–62] In their studies, deformations of the capsules in flow (inside a microfluidic device) have been estimated and confirmed dependent on capillary number change ($Ca = \mu V / \sigma$, where μ is a dynamic viscosity of the liquid, V is a characteristic velocity, and σ is a surface tension or interfacial tension between the two fluid phases.) at the same diameter of the capsules and the width of the microfluidic channels. In our study, we have gelation over time that changes the elasticity of the droplets (soft particles at the end of the gelation process) as well as not uniform hydrodynamic force as we add the second continuous phase (see Figure S6, Supporting Information). To understand those behaviors, more detailed experiments considering the parameters mentioned above have to be conducted in the future. The use of the PVCL linear is essential to form stable gels. To show the necessity of the PVCL chain, an identical synthesis without them was conducted. Figure S7 of the Supporting Information indicates CLSM images of the microgel-based colloidosomes (hollow structure) and supraballs (no-hollow structure) using the TA and different concentrations of the PVCL microgels (between 0.5 and 10 mg mL⁻¹) in the absence of the PVCL linear polymers after one-day gelation in octanol. The colloidosomes with the low concentration of the microgels (0.5–1.0 mg mL⁻¹), they show hollow architectures as expected, no uniform distribution since the droplets are merged due to the instability. As microgel concentrations increase (2.5–10 mg mL⁻¹) microparticles show less hollow morphology and the size distribution is becoming uniform. The phenomena are similar to the study of the emulsions in the first part. It is also confirmed that the microgels do not disperse in the continuous phase in the case of higher microgel concentration, unlike we have observed with emulsions in Figure 1. This proves that we could successfully entrap the microgels inside microdroplets (and at the surfaces) using the on-chip gelation of the microfluidic device. Nevertheless, the colloidosomes and supraballs synthesized without the addition of the PVCL chains are not stable after purification when they are dispersed in fresh water or EtOH. To stabilize colloidal particles, a small amount of PVCL polymers (3 mg mL⁻¹) is added to the water solution as described in Scheme 2. The morphology variations of the resulting colloidosomes and suprastructures derived from changing microgel concentrations during the microfluidic fabrication with optimized parameters (dispersed solution at pH 10.8–11.0, gelation after one day) were observed under CLSM and

listed in Figure 2. The optical images (top) and fluorescence (bottom) show the shape of the suprastructures dependent on the concentration of the microgels after one day further gelation in octanol. Generally, the synthesized soft colloidal particles show nonspherical shapes. The one with 1 mg mL⁻¹ of the microgels represents hollow buckled cone (or parachute) shape, which might be result of the hydrodynamic stress in the flow on the microfluidic device during the gelation step. Furthermore, the particles are hollow since the microgels inside the water droplets might adsorb at the interface. When the microgel concentration increases to 2.5 mg mL⁻¹, they show hollow structures, which might be resulting from self-assembly of the PVCL microgels at the surfaces as could be seen in emulsion formations only with microgels (Figure 1). To have a closer look into the structure, a widefield fluorescent image was acquired with Thunder Imager with computational clearing (Leica), which efficiently differentiates between signal and background.

The colloidosomes with the microgel concentration 2.5 mg mL⁻¹ have been chosen since they show hollow structures under confocal microscopy. The image (Figure S8, Supporting Information) presents the hollow core of the colloidosomes while the densely packed red fluorescent color is visible at the surfaces. The white dashed line in the image was used to calculate and plot the fluorescence intensity profile (inset). The intensity of the shell is significantly higher than that of the core indicating that the colloidosome has a hollow structure.^[26] Furthermore, at this microgel concentration of 2.5 mg mL⁻¹, colloidosomes are obtaining increasing stability thus, they do not deform as significantly as those with the lower concentration (1 mg mL⁻¹) of the microgels do. The deformation process can be observed during the microfluidic reaction (optical microscopy images in Scheme 2d,e and in Video S2 (1) and (2), Supporting Information). As can be seen in the videos, the spherical templates gradually developed into anisotropic colloidosomes after the droplets were leaving the second cross-junction. At a higher concentration (with 10 mg mL⁻¹), the resulted in colloidal supraballs indicate close to full structure in the CLSM image as well as less deformation of the architecture. Moreover, all synthesized suprastructures are stable after purification in water as can be seen in bright field and fluorescence images in CLSM (Figure S9, Supporting Information). This experiment clearly shows that the amount of the PVCL microgels inside water precursor droplets has an influence on their stability during the on-chip fabrication process, which can give control over the shape resulting from the gelation of the precursor droplets. The chemical composition of the colloidosomes (with 2.5 mg mL⁻¹ of the microgels) has been analyzed via FTIR (Figure S10, Supporting Information). The strong absorption band at 1615 cm⁻¹ (PVCL linear chain) and 1616 cm⁻¹ (PVCL-BIS microgels) corresponds to carbonyl stretching vibrations of the caprolactam ring of the PVCL polymers. In colloidosomes, the peak overlaps with carbon–carbon stretching vibrations of the aromatic rings of TA (1608 and 1517 cm⁻¹).^[63] Furthermore, the peak at 1718 cm⁻¹ of the colloidosomes is associated with carbonyl stretching vibration of the ester groups in TA molecules in presence of hydrogen bonds.^[64] Those characteristic peaks of the colloidosomes indicate the chemical composition of the PVCL linear chain, PVCL-BIS microgels and TA as well as the formation of the hydrogen bonds. To check the influence of flow

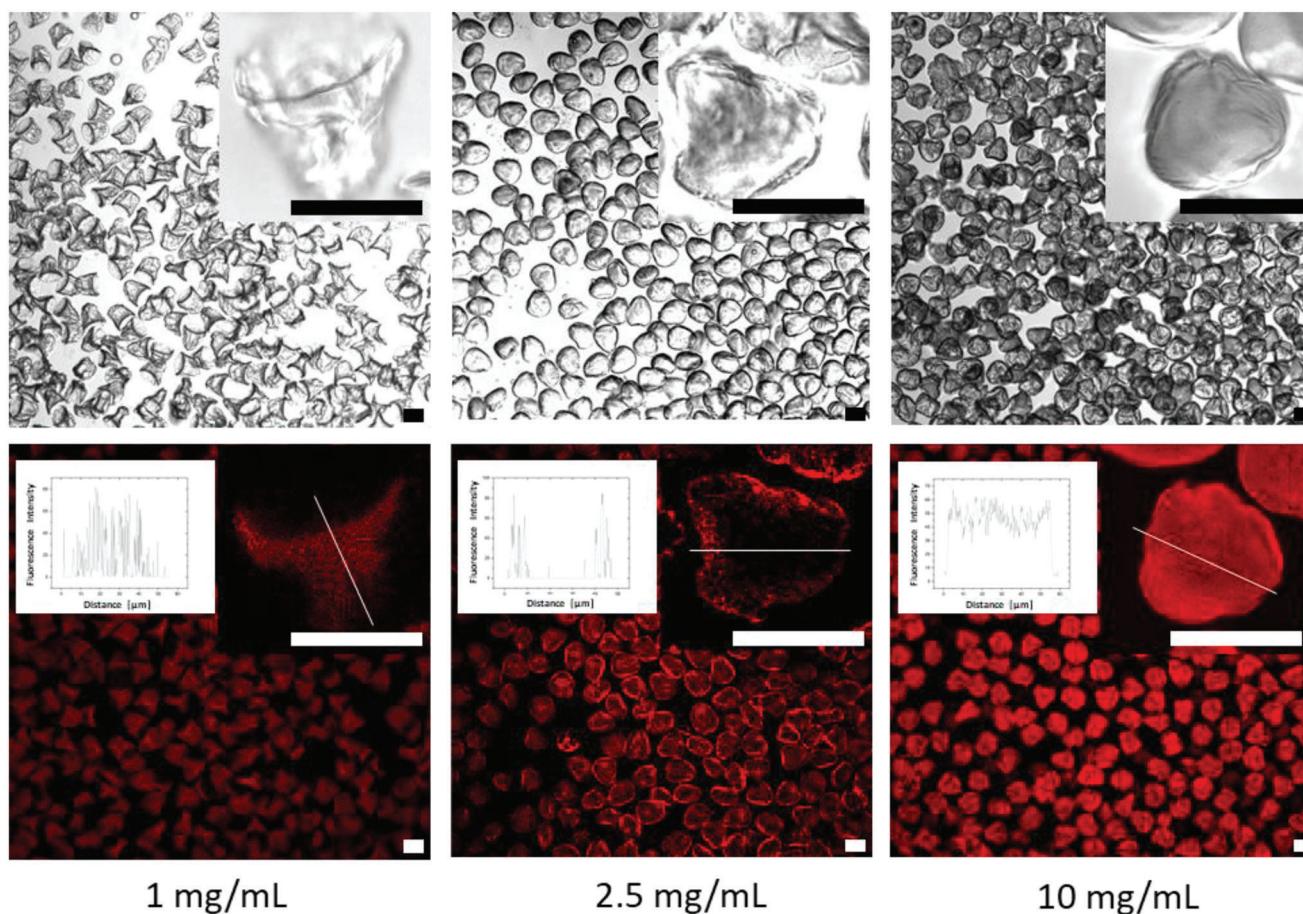


Figure 2. Bright field images (top) and fluorescence images (bottom) by CLSM show the synthesized colloidal particles with different microgel concentrations in octanol one day after the synthesis. Insets show fluorescence intensity profiles, which are derived from cross-sections of the fluorescence images. All scale bars represent 50 μm (images using the $\times 10$ objective and the images of the insets are recorded using the $\times 63$ objective).

rates on morphologies of obtained structures during on-chip gelation, the flow rate of the water phase was increased to 150 $\mu\text{L h}^{-1}$. Previous other studies^[65–67] reported that the viscosity changes in the dispersed phase in microfluidics flow focusing devices play an important role in the emulsification as well as in the droplet formation and break-up mechanism. The dispersed phase in the present study contains the PVCL chain, the PVCL microgels as well as the TA. Those molecules (between the TA and the PVCL) form supramolecular interactions (hydrophobic interactions) even though the preparation was conducted at high pH (10.8–11) where most of the TA were deprotonated meaning the absence of the hydrogen bonds. Therefore, it is expected that the flow rate increase of the dispersed phase results in different sizes in comparison to that of emulsions studied in the first part (Figure 1; Figures S4 and S5, Supporting Information). The soft supraballs with the PVCL microgels (10 mg mL^{-1}) were formed with two different flow rates of the water stream with 50 and 150 $\mu\text{L h}^{-1}$. After purification, they are redispersed in fresh water and the colloidal suprastructures synthesized with both flow rates are presented in the optical microscopy images in Figure 3a,b. There is a clear morphology change from the low to the high flow rate and in the latter case, rod-shaped

supraparticles with aspect ratio of 1.81 could be obtained. Also, the gels with different concentrations of the microgels show a rod-shape in CLSM (Figure S11, Supporting Information) while the hollow morphology is not visible. In the previous study, the method to synthesize rod-shaped supramolecular microgels based on hydrogen bonds between the PVCL linear polymers and the TA was presented.^[41] There, higher polymer concentration (PVCL) was necessary (150 mg mL^{-1}) to hold the nonspherical shapes. It is noticeable that the on-chip microfluidic method combining the PVCL linear polymer, the PVCL microgels, and the TA lead to the formation of the stable rod-shaped microgels with significantly lower concentrations. This might lead to the notable alternation of the elastic and mechanical properties of the microgels such as stiffness, elasticity, and rigidity,^[68,69] which might play an important role in different fields such as biomedical applications.^[70]

Moreover, we varied the flow rate of the continuous phases to evaluate their functions. In Figure 3c,d, images represent soft particles on outlet directly after gelation in octanol. In both cases (1 and 10 mg mL^{-1}), the length of the particles increase with decreasing the flow rate of the continuous phases as the capillary number decreases (only the velocity of the dispersed phase

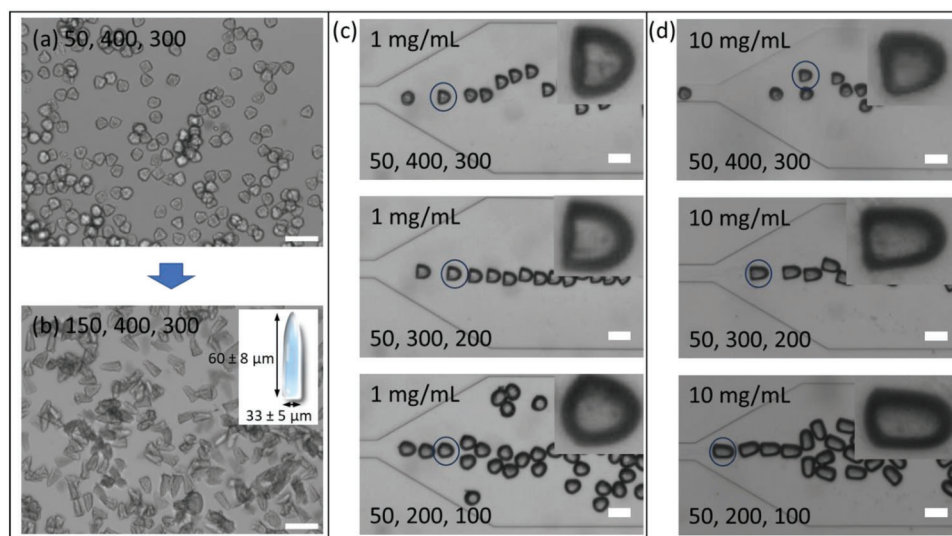


Figure 3. Shape modulation by varying flow rates. a,b) Optical microscopy images of the spherical- and rod-shaped soft colloidal particles synthesized with different flow rates of water stream ($50 \mu\text{L h}^{-1}$ for (a) and $150 \mu\text{L h}^{-1}$ for (b)) with 10 mg mL^{-1} of the PVCL microgels) after purification in water. The image in panel represents the rod-shaped structure with width and length. 20 random particles are measured and the standard deviation is provided. c,d) Optical images of the formed colloidal structure with different PVCL microgel's concentration and flow rates of the dispersed phases on the outlet direct after the synthesis in octanol. The flow rates are addressed in the order: (the dispersed phases, the first continuous phases, the second continuous phases) in $\mu\text{L h}^{-1}$. In the panel on each of images, magnified image of the particles in blue circles are presented. The scale bars represent $100 \mu\text{m}$.

increases while the interfacial tension between dispersed phase and first continuous phase and viscosity of the dispersed phases keep the same).^[71,72] We assume that the volume of the microdroplets are set at the first cross-junction where droplets are formed. Another interesting factor is the buckling behaviors during the gelation. With 1 mg mL^{-1} particles, greater deformation at higher flow rates of the continuous phases could be observed while that with 10 mg mL^{-1} does not seem significance. This experiment clearly indicates that the length of the asymmetrical shape can be varied with different volume of the microdroplets/particles and the flow rate of the second dispersed phase has also impact on the deformations besides microgel's concentrations.

2.3. Properties of the Colloidosomes

The structure of the colloidosomes with 2.5 mg mL^{-1} of the microgels after the purification was observed further under field emission scanning electron microscopy (FESEM) in a dry state and cryo-field emission scanning electron microscopy (cryo-FESEM) in a frozen state. The images (Figure 4a) indicate a colloidosome shrink under vacuum and crumpling surface morphology, characteristic of a soft microcapsule in a dry state.^[26,73] It is noteworthy that on the FESEM images of the supramolecular microgels that were synthesized from only the PVCL chain and the TA (in the absence of the microgels) do not show that crumpled surface.^[41] Furthermore, no clear single microgel structure is visible in the insets but only homogeneous polymer layers. This can be explained that the PVCL microgels being bonded by the TA and the PVCL linear polymers which might stretch microgels on the surfaces. More detailed inside structure of the colloidosomes could be observed via a cryo-FESEM technique

(Figure S12, Supporting Information). The image shows that a void space is present inside the particle, however, some polymer fractions can also be detected and the particle do not show a well-defined core-shell structure. This might be due to the fact that some PVCL chains are linked by TA inside microdroplets without PVCL microgels that absorb at the surfaces. The PVCL-based microgels synthesized by precipitation polymerization show thermoresponsiveness with their VPTT (Figure S2, Supporting Information). However, in the presence of the TA the resulting PVCL-based suprastructures do not show the thermoresponsiveness between 20 and $50 \text{ }^\circ\text{C}$ (Figure S13, Supporting Information) as observed in our previous studies with PVCL-TA microgels.^[41,43] This might be due to the fact that the formation of the hydrogen bonds between the TA and PVCL chains might interrupt interactions between the polymers and the water molecules. To estimate the porosity of the colloidosomes, diffusion study using different molecular weights of FITC-Dex (4 , 40 , and 500 kDa) was performed (Figure 4b). These polymers are known to present a globular structure in water with hydrodynamic diameters of 3.3 , 8.7 , and 28.8 nm , respectively.^[74] CLSM was used to examine the dextran diffusion inside the colloidosomes in water as presented in different previous works (Figure 4c).^[75,76] Permeability is represented as ratio of fluorescence intensity in the colloidosomes and the surrounding water solution. In case of 4 and 40 kDa FITC-Dex, the fluorescence intensity inside the colloidosomes and in water shows no differences whereas with 500 kDa shows a dissimilarity of the fluorescence intensity is visible. This indicates that the pore sizes of the colloidosomes might be between 8.7 and 28.8 nm . The colloidosomes are formed by interlinking microgels by hydrogen bonds. Therefore, breaking the interlinks by pH-change is expected to trigger cleavage of the colloidosomes. Figure 5a shows the optical images of the disassembly process of the colloidosomes with 2.5 mg mL^{-1} of the

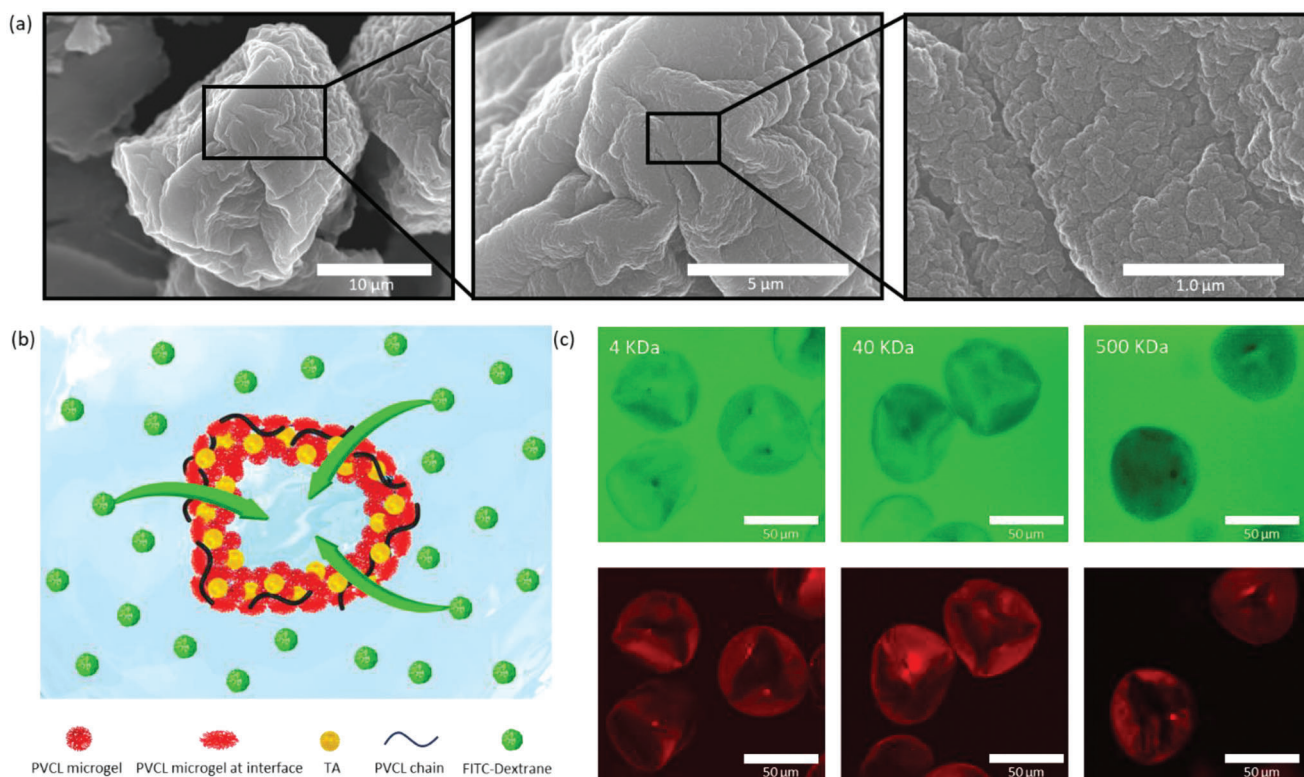


Figure 4. a) FESEM images of the colloidosomes synthesized with 2.5 mg mL^{-1} microgels. b) The schematic illustration of diffusion study with a colloidosome in the presence of FITC-dextran. c) The CLSM images during incubation in water in the presence of FITC-dextran with three different molecular weights (4, 40, and 500 kDa). Images on top show green fluorescence pointing out the FITC-dextran, and those on the bottom depict red fluorescence indicating the microgels labeled with Rhodamine B inside the colloidosomes.

microgels by time as illustrated in the image (b). The colloidosomes are disassembled by adding a basic buffer (pH = 11) (Video S3, Supporting Information). The hydrodynamic radius of the microgels after the disassembly at pH 11 shows $87 \pm 4 \text{ nm}$ with $\text{PDI} = 0.16 \pm 0.02$ by DLS (b), which indicates similar sizes of the microgels before the fabrications (compare with Figure S1 and Table S1, Supporting Information). On the other hand, in acidic and neutral conditions (pH = 3, 5, and 7), colloidosomes are stable in the buffer solution. We used the same ionic strength of 10 mM of the buffers in order to examine solely the influence of the pH values on the structure stabilities (Figure S14, Supporting Information). This unique property of our microgel-based colloidosomes could be studied further for the multi-component microreactors as published in recent years.^[77,78] The principle is that two or more separated colloids can build a larger unit while preserving their functions and structures.^[77,79,80] This flexible strategy can be extended to the gels containing other cargoes, for example, with a series of enzymes for multicompart microreactors as cell mimics.^[81,82] With other methods, the realization requires either multiple emulsification steps to generate double emulsion droplets or additional postchemical reactions to form the compartments which are quite complex and time consuming steps.^[83,84]

In this part, we are demonstrating multicompartmentalization in our microgel-based colloidosomes. Another batch of PVCL microgels was synthesized and labeled with FITC in addition to the PVCL microgels labeled with Rhodamine B which are uti-

lized to synthesize suprastructures already. The hydrodynamic radius of the new microgels is 343 nm (Table S2 and Figure S15, Supporting Information). For the multicompartmentalized colloidosomes, both of the PVCL microgels in a 1:1 weight ratio are mixed in the preparation of the dispersed phases. After the purification, CLSM images are recorded in fresh water (Figure 5d). With both lasers (488 nm for FITC and 561 nm for Rhodamine B), expected fluorescence emitted light is detected. Merging both fluorescence images indicates that both of the microgels are distributed in the colloidosomes homogeneously. The multicompartmentalized colloidosomes are cleaved in a basic condition (in pH = 11 buffer) (c). In the DLS measurement, two different sizes (≈ 100 and 360 nm) are visible, which indicates the two initial microgels. This experiment demonstrates the simplicity of the fabrication for building a larger unit with two or more separated colloids as well as obtaining the single particles after the cleavage that can be studied further for designing complexed materials.

3. Conclusion

In this study, a straightforward on-chip fabrication of nonspherical microgel-based suprastructures was demonstrated. The ability of the PVCL microgels to self-assemble at the liquid–liquid interfaces combined with interparticle supramolecular cross-linking enables to control over the morphology and properties of the colloidal suprastructures.

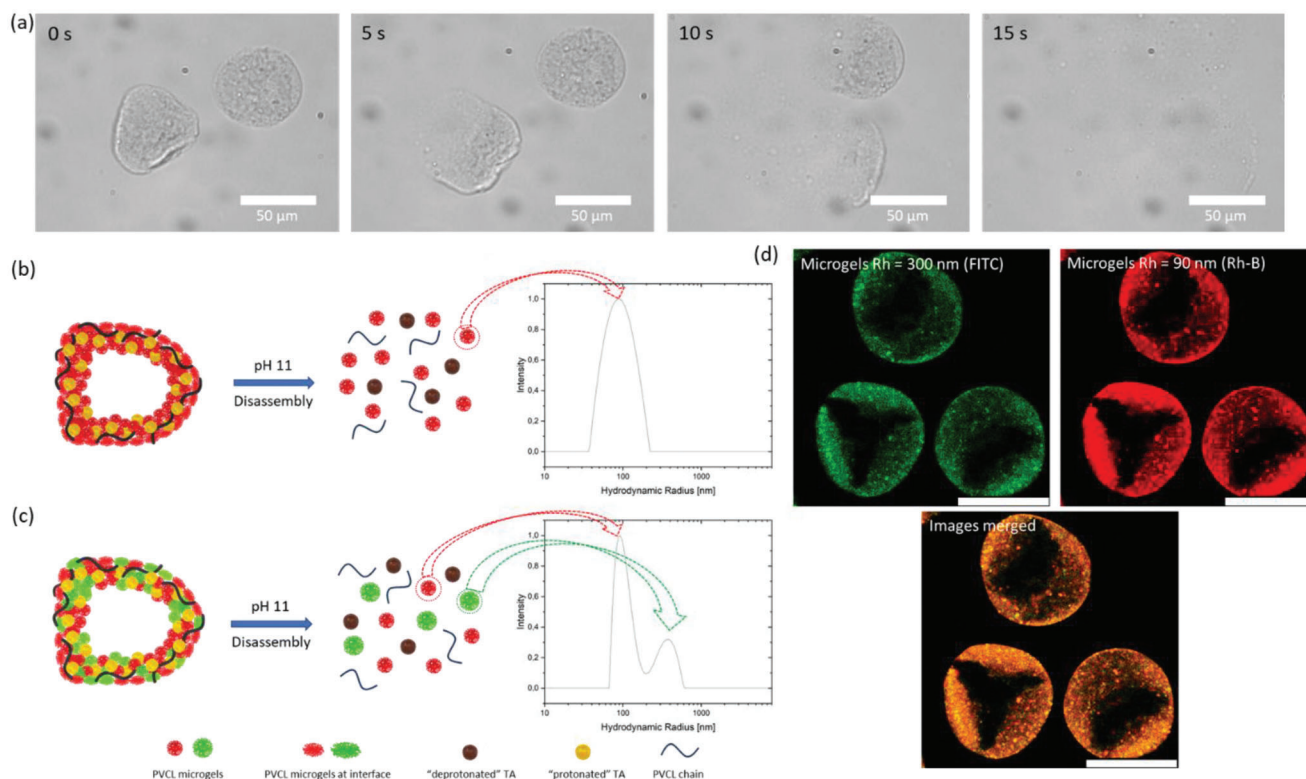


Figure 5. a) Optical images of the disassembly in an alkaline condition of the colloidosomes with 2.5 mg mL^{-1} of the PVCL microgels (see Video S3, Supporting Information). b) Schematic illustration of the disassembly of the colloidosomes and size distribution of the disassembled solution at pH 11 by DLS. c) Schematic illustration of the disassembly of the supramolecular multicompartmentalized colloidosomes and the size distribution after disintegration at pH 11 by DLS. d) CLSM images detect emission from the different microgels.

First, the PVCL microgels (hydrodynamic radius 92 nm, PDI = 0.16) with 2.5 mol% BIS as cross-linker and labeled with a fluorescent active dye (Rhodamine B) were successfully synthesized. Following this step, water (containing the PVCL microgels) in oil (octanol) emulsions were formed on a microfluidic device and the localization of the microgels in the system was studied. Self-assembly of the microgels at the liquid–liquid interfaces could be observed for all concentrations of the microgels (0.5 to 20 mg mL^{-1}). Moreover, unstable droplets with broader size distribution were formed when low concentrations of the microgels were used. Contrary, at high microgel concentrations droplets exhibit uniform sizes (96 – $103 \mu\text{m}$) and were stable in octanol. There were no significant size differences of the droplets formed with microgel concentrations between 2.5 and 20 mg mL^{-1} indicating that the presence of the microgels did not play a crucial role in the early stages of the emulsion formation dynamics (at the first cross-junction in Scheme 1). The microgels influence, however, the stability of the droplets indicating that they might adsorb at the interfaces after the formation of the droplets. Furthermore, when the microgels cover the surfaces of the droplets they preferably disperse in the octanol fluid, which is a type of polar organic solvent.

In the next part, different types of the nonspherical suprastructures were synthesized using on-chip gelation. Different parameters were altered such as microgel concentrations and flow rates. By changing microgel concentrations, the buckled shaped (1 mg mL^{-1}), hollow (2.5 mg mL^{-1}) colloidosomes and full supraballs

(10 mg mL^{-1}) were formed. Varying the flow rates (dispersed and continuous phases) enabled additional particle's deformation as well as alternation on the lengths of the rod-shaped supraparticles. The colloidosomes synthesized with 2.5 mg mL^{-1} microgels were used for further studies and their hollow structures could be proven by different microscopy techniques. The synthesized colloidosomes were disassembled at an alkaline condition (pH 11) within 20 s and disintegrated into the initial microgels. This unique property of our colloidosomes could be studied further for the multicomponent microreactors as published in recent years.

As perspective, controlling further the gelation process would lead to fine-tuning the hollow-shell structures by varying thickness of the shells. Nevertheless, considering the noncovalent nature of the microgel networks, hollowness, controllable nonspherical shape and pH-degradable property, this technology can become a powerful tool for the fabrication of compartmentalized soft materials for different bio-, food-, and medical applications.

4. Experimental Section

Materials: PVCL was obtained from BASF as Luviskol (30% in EtOH and Isopropanol). The number average molecular weight (M_n) was determined using GPC and is $\approx 27\,500 \text{ g mol}^{-1}$. Alcohol contained in the product was removed using rotary evaporator and lyophilization before use. TA (99.5% \leq), acetic acid (99.8% \leq), 2,2-azobis(2-methylpropionamide) (AMPA, 97%), *N*'-methylenebisacrylamide (BIS, 99%), fluorescein-O-

acrylate (95%), Span 80 (60% \leq), and *N*-vinylcaprolactam (VCL, 98% stabilized) silicone isolators, press-to-seal (8 well, 0.5 mm \times 9 mm, silicone/silicone, round), 1 M of sodium hydroxide (NaOH), ethanol (EtOH, 99.8%), water (HPLC), Span 80 (\geq 60%), fluorescein-isothiocyanat isomer I (FITC, \geq 90%), 1-Octanol (\geq 99%), 1 M of phosphoric acid, natriumphosphat (NaH₂PO₄, \geq 99%), disodium hydrogen phosphate (Na₂HPO₄, \geq 99%), potassium hydroxide (KOH, \geq 85%), and monopotassium phosphate (KH₂PO₄, \geq 99%) were purchased from Sigma-Aldrich. VCL was purified by distillation in vacuo and subsequent recrystallization from hexane. Methacryloxyethyl thiocarbamoyl Rhodamine B (Rhodamine B, 95–100%) was obtained from Polysciences. All of the reactants were used without further purifications. HFE (Novac 7500) was obtained from 3M and Krytox 157 FSH was purchased from Chamours. Silgard 184 kit was purchased from Dow Corning. PE Tubing (ID = 0.38 mm, OD = 1.98 mm) was obtained from Smiths Medical. Aquapel was provided from Schutzprofi. Sampling tool (type 0.75 mm) was obtained from EMS-Core.

Device Fabrication: Microfluidic devices were fabricated by soft lithography. AutoCAD (Autodesk, USA) software was used to design the microfluidic channel in a 2D drawing, which was printed on a high-resolution (25 000 dpi) dark-field photomask. Photolithography was applied to pattern an epoxy-based photoresist (SU-8) on a silicon wafer using the printed photomask as template. Soft lithography on the patterned silicon wafer was used to produce PDMS-based microfluidic devices. Briefly, Silgard 184 kit was employed to prepare a mixture containing 1 part of curing agent and 10 parts of PDMS base. The mixture was poured on the previously prepared silicon wafer and excess of air was removed under high vacuum for 1 h. The system was heated at 65 °C overnight before the cured PDMS mold was peeled off from the silicon wafer. The PDMS mould and a glass slide were treated with oxygen plasma and covalently bound together via a condensation reaction. The device was heated at 65 °C for total completion of the bonding for 1 h. After finalization of the bonding process of the PDMS to the glass slide, the silane (Aquapel) was used to render the microfluidic channels hydrophobic. The device was placed in a high-vacuum desiccator with 200 μ L of the silane and left overnight to enable the chemical vapor deposition of the silane and its consequent covalent bond to the surface of the channels, after which it was heated at 65 °C for 1 h.

General Workflow for Microfluidic Devices: Microfluidic experiments were conducted on a microfluidic station consisting of two syringe pumps (PHD Ultra, Harvard Apparatus, Holliston, MA, USA), to control the flow rates of the two different phases. An inverted microscope (Motic AE2000, TED PELLA, INC., Redding, CA) equipped with a camera (Flea3, Point Grey, Richmond, CA) was applied to observe flow and droplet formation. The PDMS microfluidic device was connected to the system using fine bore polyethylene tubing. The microchannels had a rectangular cross-junction with a uniform height of 80 μ m.

Synthesis of the PVCL Microgels and the Labelings with Fluorescent Dyes: Microgel preparation was carried out by the free-radical precipitation polymerization method. Recrystallized (with hexane) VCL (1.56 g, 11.3 mmol, 97.5 mol%) as monomer, the cross-linker BIS (45 mg, 0.29 mmol, 2.5 mol%), and the fluorescent dye Rhodamine B (7.5 mg, 0.1 mol%, for the microgels to label with FITC for multicompartmentalization no Rhodamine B was incorporated) were added to 73 mL of the HPLC water in a 100 mL round bottom flask. In a separate snap cap tube, the initiator AMPA (5.66 mg, 0.02 mmol, 0.16 mol%, for the microgels to label with FITC for multicompartmentalization: 56.6 mg, 0.2 mmol, 1.6 mol%) was mixed with 2 mL of the HPLC water. Both reaction vessels were degassed with nitrogen for 45 min at 70 °C. Then the aqueous AMPA solution was added to the mixture of monomers and reacted for 3 h or the purification of the microgels, a ZelluTrans dialysis tube (12–14 kDa) was used to remove unreacted reactants and not cross-linked polymers. Dialysis was performed for seven days in a 5 L beaker against distilled water. The water was changed daily twice. The microgel solution was protected from light via aluminum foil. The remaining solvent was removed by freeze-drying with the LyoQuest laboratory freeze dryer. For this purpose, the microgel dispersion was first frozen using liquid nitrogen and then completely dried for three days. Second microgels for the multicompartmentalized colloidosomes were synthesized with 1.6 mol% AMPA. They were labeled further with FITC. For this, 10 mL of the microgel solution after the purification

step was mixed with fluorescein-isothiocyanat isomer I (2.0 mmol, 10 equiv. to AMPA) and stirred at RT for two days. For purification, the mixture was dialyzed against distilled water for seven days in a 5 L beaker and the mixture was covered by aluminum foil for storage.

Study of the Microgel's Behavior at Emulsions: A solution of 1-octanol with 2 vol% of Span 80 as stabilizer was used as the oil phase and transferred into 10 mL of the glass syringe. The addition of the oil phase was done via the 10 mL glass syringe in combination with the syringe pump at a flow rate of 300 μ L h⁻¹. For the aqueous solution the microgel concentration (0.5, 1.0, 2.5, 5.0, 7.5, 10.0, 15.0, 20.0 mg mL⁻¹) was adjusted by addition of the HPLC water. The solution was dispersed by ultrasonification for 5 min and filtered using a syringe filter (1.20 μ m, filter- ϕ : 25 mm). The addition was carried out with a 1 mL of glass syringe in combination with the Syringe pump. Flow rates of 50 and 150 μ L h⁻¹ were used for the dispersed phases. The resulted emulsions were corrected in a vial using PE tubing and the emulsion was observed directly under CLSM to check the behavior of the microgels.

Synthesis of the Nonspherical Suprastructures: Two continuous phases and one dispersed phase were used for the nonspherical colloidosomes and gel synthesis. The preparation of the first oil phase was conducted with 1-octanol and 2 vol% of Span 80. The second oil phase contained 1 vol% of acetic acid in octanol. The addition of the oil phases was done via the 10 mL glass syringes in combination with the syringe pumps. The flow rate for the first oil (continuous) phase is 400 μ L h⁻¹ and for the second oil (continuous) phase 300 μ L h⁻¹ unless no additional information had been given. To prepare the aqueous phase, a solution of TA (32.0 mg, 16.0 mg mL⁻¹) was first prepared with 2 mL of the HPLC water in a 3 mL snap cap tube and degassed with argon for 5 min to avoid oxidation of TA. Then the pH was adjusted with NaOH to 10.8–11. Under argon conditions, the PVCL microgels were added according to the desired concentration (1.0, 2.5, and 10.0 mg mL⁻¹ and for the multicompartmentalized particle 1:1 ratio of two types of the microgels and the sum is 2.5 mg mL⁻¹) and PVCL-chains (6.0 mg, 3.0 mg mL⁻¹). Homogeneous distribution of the reactants in the solution was achieved by shaking three times on the rotex shaker followed by 5 min of ice-cooled ultrasonification. Under inert gas, the solution was filtered with a syringe filter (1.20 μ m, filter- ϕ : 25 mm) and transferred to the 1 mL glass syringe. Flow rates of 50 and 150 μ L h⁻¹ were used for the dispersed phases.

DLS Measurements of the PVCL Microgels: The microgel characterization via DLS was performed using an ALV/CGS-3 Compact Goniometer System with an ALV/LSE 5004 Tau Digital Correlator and a JDS Uniphase laser operation at 632.8 nm. A fixed scattering angle of $\theta = 90^\circ$ was used. Before the measurements, the microgel samples were filtered through a syringe filter (polyester) with a pore size of 1.2 μ m, and the solid concentration was set to 0.1 mg mL⁻¹ with HPLC grade water. Single measurement was carried out at 20 °C.

Scanning Electron Microscopy Measurements: For the FESEM measurements, the microgel solution was air-dried under ambient conditions on carbon grids (Carbon Film 200 Mesh Copper Grids, Electron Microscopy Sciences). Ultrahigh Resolution Scanning Electron Microscope SU9000 (Hitachi-High Technologies) was used for the measurements. The cryo-FESEM measurement was carried out using the S4800 FESEM by Hitachi-High Technologies. A drop of microgel solution was placed in metal rivets (or tubes) and frozen in liquid nitrogen. The rivets containing the frozen sample were inserted into the electron microscopcope under vacuum while keeping the same temperature in their frozen state. Before the measurement a sublimation process was executed on the top surface of the sample. The sample was uncovered from the surrounding ice by \approx 2–4 nm in depth, allowing a better view on the colloidosomes. The measurement was done by using the secondary electron-detector at an accelerating voltage of 1 kV and an emission current of \approx 2 μ A. The scanning electron microscopy experiment was performed by Stefan Hauk at DWI–Leibniz Institute for Interactive Materials.

Thermoresponsiveness Study via Optical Microscopy: Images for thermoresponsiveness of microgels were recorded using a microscope (Axioptan 2, Zeiss). A drop of the colloidosome solution was placed in a silicon isolater that was placed between two glass slides and the measurement was performed. Two optical images were taken once at 20 °C and

the other one at 50 °C. For temperature control, a self-made hot plate with polyimide Thermofoil™ heaters, PT100 IEC 751 tolerance class 1/3B temperature sensor, and LakeShore Model 330 Autotuning Temperature Controller (Lake Shore Cryotronics, Inc., USA) were used.

CLSM Images: 20 µL of the solutions was placed in a glass slide with a silicone isolator and performed the measurements. CLSM imaging was performed using a TCS SP8 setup from Leica Microsystems. The fluorescein moieties incorporated in the microgels was excited using an Argon Laser filtered to a wavelength of 488 nm. The resulting fluorescent emission was detected using a HyD detector in the range of 500–550 nm. The Rhodamine B moieties incorporated in the microgels were excited using a visual light filtered to a wavelength of 561 nm. The resulting fluorescent emission was detected using a HyD detector in the range of 575–610 nm. For the imaging two main objectives were used: 1) HCX PL Fluotar 10×/0.30 (air) and 2) HC PL APO 63×/1.40 Oil CS2.

Preparation of the Buffer Solutions: For the buffer solutions, stock solutions were prepared and then mixed with proper amount. For pH 3 buffer, 0.23 mL of phosphoric acid (1 M), 0.074 mL of NaCl (1 M), 0.1 g of sodium phosphate, and 99.7 mL of HPLC water were mixed. For the pH 5 buffer, 38.12 mL of succinic acid solution (0.02 M), 16.8 mL of KOH (0.05 M), and 45.08 mL of HPLC water were mixed. For the pH 7 buffer, 13.96 mL of monophosphate potassium phosphate (0.02 M), 24.05 mL of monosodium phosphate, and 62 mL of HPLC water were mixed.

FTIR Measurements: The chemical composition of the colloidosomes was characterized by ATR-FTIR spectroscopy on a PerkinElmer Spectrum 3 equipped with a GladiATR diamond frontier. All measurements were performed within a spectral range from 4000 to 400 cm⁻¹ with a spectral resolution of 4 cm⁻¹ and a sample scan time of 4 scans at room temperature. The data analysis was carried out with the software Spectrum (Version 10.7.1) from PerkinElmer. For the measurements, the colloidosomes solution (100 µL) was dried in an oven over night. The dried sample was transferred on ATR of the FTIR for the measurements.

GPC Measurement: Number-average molecular weights (\bar{M}_n), weight-average molecular weights (\bar{M}_w), and dispersities ($D, \bar{M}_w/\bar{M}_n$) were determined by GPC using dimethylformamide (DMF) as an eluent for the PVCL homopolymer. The measurements of the samples dissolved in DMF were performed using an Agilent 1260 infinity system equipped with a refractive index detector (SECURITY², PSS). The eluent contained 1 g l⁻¹ lithium bromide (LiBr, ≥99%, Sigma-Aldrich). The solvent of the samples contained traces of toluene as an internal standard. The used sample concentration was ≈5 mg mL⁻¹. One precolumn (8 mm × 50 mm) and three PSS GRAM gel columns (8 mm × 300 mm, Polymer Standards Service) were used at a flow rate of 1.0 mL min⁻¹ at a temperature of 60 °C. The diameter of the gel particles was 10 µm, and the nominal pore widths were 30, 1000, and 1000 Å. Calibration was achieved using narrow distributed poly methyl methacrylate standards. The results were evaluated using the PSS WinGPC UniChrom software (Version 8.3.2).

Supporting Information

Supporting Information is available from the Wiley Online Library or from the author.

Acknowledgements

The authors thank Dr. Tamas Harászti and Stefan Hauk for help with electron- and optical microscopy measurements and Pablo Radermacher und Jan Schumacher for recording a beautiful image of the colloidosomes with Leica Thunder. Hannah Mathews and Maria Pieper are acknowledged for the preparation of the buffer salutation. The authors thank Selin Bulut for the help with a microfluidic device preparation and Susanne Braun for the GPC measurement. The authors also thank to Hye Ji Lee for graphical abstract and image design of the figures. Financial support of the Deutsche Forschungsgemeinschaft (DFG) within Collaborative Research Center SFB 985 “Functional Microgels and Microgel Systems” is gratefully acknowledged. This work was performed in part at the Center for Chem-

ical Polymer Technology (CPT), which was supported by the EU and the federal state of North Rhine–Westphalia (Grant No. EFRE 30 00883 02). Open access funding enabled and organized by Projekt DEAL.

Conflict of Interest

The authors declare no conflict of interest.

Data Availability Statement

The data that support the findings of this study are available from the corresponding author upon reasonable request.

Keywords

colloidal suprastructures, colloidosomes, microfluidics, microgels, pH-responsive, supramolecular chemistry

Received: April 24, 2023

Revised: July 25, 2023

Published online:

- [1] R. Aveyard, B. P. Binks, J. H. Clint, *Adv. Colloid Interface Sci.* **2003**, *100*, 503.
- [2] B. P. Binks, T. S. Horozov, *Colloidal Particles at Liquid Interfaces*, Cambridge University Press, Cambridge **2006**.
- [3] W. Ramsden, F. Gotch, *Proc. R. Soc. London, Ser. B* **1904**, *72*, 156.
- [4] S. U. Pickering, *J. Chem. Soc. Trans.* **1907**, *91*, 2001.
- [5] L. M. Croll, H. D. H. Stöver, *Langmuir* **2003**, *19*, 5918.
- [6] T. Chen, P. J. Colver, S. A. F. Bon, *Adv. Mater.* **2007**, *19*, 2286.
- [7] H. N. Yow, A. F. Routh, *Langmuir* **2009**, *25*, 159.
- [8] Q. Yuan, O. J. Cayre, S. Fujii, S. P. Armes, R. A. Williams, S. Biggs, *Langmuir* **2010**, *26*, 18408.
- [9] K. L. Thompson, S. P. Armes, J. R. Howse, S. Ebbens, I. Ahmad, J. H. Zaidi, D. W. York, J. A. Burdiss, *Macromol. Chem.* **2010**, *43*, 10466.
- [10] A. Walsh, K. L. Thompson, S. P. Armes, D. W. York, *Langmuir* **2010**, *26*, 18039.
- [11] O. D. Velev, K. Furusawa, K. Nagayama, *Langmuir* **1996**, *12*, 2374.
- [12] A. D. Dinsmore, M. F. Hsu, M. G. Nikolaides, M. Marquez, A. R. Bausch, D. A. Weitz, *Science* **2002**, *298*, 1006.
- [13] H. Wang, X. Zhu, L. Tsarkova, A. Pich, M. Möller, *ACS Nano* **2011**, *5*, 3937.
- [14] J. Wu, G.-H. Ma, *Small* **2016**, *12*, 4633.
- [15] S. Sun, M. Li, F. Dong, S. Wang, L. Tian, S. Mann, *Small* **2016**, *12*, 1920.
- [16] Y. Gong, A. M. Zhu, Q. G. Zhang, M. L. Ye, H. T. Wang, Q. L. Liu, *ACS Appl. Mater. Interfaces* **2013**, *5*, 10682.
- [17] A. J. Morse, J. Madsen, D. J. Gowney, S. P. Armes, P. Mills, R. Swart, *Langmuir* **2014**, *30*, 12509.
- [18] Y. Hu, J. Pérez-Mercader, *ACS Appl. Nano Mater.* **2018**, *1*, 3346.
- [19] R. Langer, N. A. Peppas, *AIChE J.* **2003**, *49*, 2990.
- [20] A. S. Hoffman, *J. Controlled Release* **1987**, *6*, 297.
- [21] T. Jung, W. Kamm, A. Breitenbach, E. Kaiserling, J. Xiao, T. Kissel, *Eur. J. Pharm. Biopharm.* **2000**, *50*, 147.
- [22] H. Zhang, S. Mardiyani, W. C. Chan, E. Kumacheva, *Biomacromolecules* **2006**, *7*, 1568.
- [23] D. B. Lawrence, T. Cai, Z. Hu, M. Marquez, A. D. Dinsmore, *Langmuir* **2007**, *23*, 395.
- [24] S. Berger, H. Zhang, A. Pich, *Adv. Funct. Mater.* **2009**, *19*, 554.

- [25] G. Agrawal, A. Ülpenich, X. Zhu, M. Möller, A. Pich, *Chem. Mater.* **2014**, *26*, 5882.
- [26] R. K. Shah, J.-W. Kim, D. A. Weitz, *Langmuir* **2010**, *26*, 1561.
- [27] P. Garstecki, M. J. Fuerstman, H. A. Stone, G. M. Whitesides, *Lab Chip* **2006**, *6*, 437.
- [28] A. S. Utada, E. Lorenceau, D. R. Link, P. D. Kaplan, H. A. Stone, D. Weitz, *Science* **2005**, *308*, 537.
- [29] A. S. Utada, L. Y. Chu, A. Fernandez-Nieves, D. R. Link, C. Holtze, D. A. Weitz, *MRS Bull.* **2007**, *32*, 702.
- [30] L. Y. Chu, A. S. Utada, R. K. Shah, J. W. Kim, D. A. Weitz, *Angew. Chem.* **2007**, *119*, 9128.
- [31] A. Abate, D. Weitz, *Small* **2009**, *5*, 2030.
- [32] J. Zhang, R. J. Coulston, S. T. Jones, J. Geng, O. A. Scherman, C. Abell, *Science* **2012**, *335*, 690.
- [33] Z. Yu, Y. Lan, R. M. Parker, W. Zhang, X. Deng, O. A. Scherman, C. Abell, *Polym. Chem.* **2016**, *7*, 5996.
- [34] L. Yang, Z. Zhou, J. Song, X. Chen, *Chem. Soc. Rev.* **2019**, *48*, 5140.
- [35] A. Donev, I. Cisse, D. Sachs, E. A. Variano, F. H. Stillinger, R. Connelly, S. Torquato, P. M. Chaikin, *Science* **2004**, *303*, 990.
- [36] J.-W. Kim, R. J. Larsen, D. A. Weitz, *Adv. Mater.* **2007**, *19*, 2005.
- [37] D. Lee, D. A. Weitz, *Small* **2009**, *5*, 1932.
- [38] F. Pignon, A. Magnin, J.-M. Piau, *J. Rheol.* **1998**, *42*, 1349.
- [39] S. M. Jogun, C. F. Zukoski, *J. Rheol.* **1999**, *43*, 847.
- [40] P. F. Noble, O. J. Cayre, R. G. Alargova, O. D. Velev, V. N. Paunov, *J. Am. Chem. Soc.* **2004**, *126*, 8092.
- [41] S. H. Jung, S. Bulut, L. P. B. Busca Guerzoni, D. Günther, S. Braun, L. De Laporte, A. Pich, *J. Colloid Interface Sci.* **2022**, *617*, 409.
- [42] H. Vihola, A. Laukkanen, L. Valtola, H. Tenhu, J. Hirvonen, *Biomaterials* **2005**, *26*, 3055.
- [43] C. M. López, A. Pich, *Macromol. Rapid Commun.* **2018**, *39*, 1700808.
- [44] A. Pich, W. Richtering, in *Chemical Design of Responsive Microgels* (Eds: A. Pich, W. Richtering), Springer, Berlin **2011**, pp. 1–37.
- [45] W. Richtering, *Langmuir* **2012**, *28*, 17218.
- [46] G. Liu, X. Li, S. Xiong, L. Li, P. K. Chu, K. W. K. Yeung, S. Wu, Z. Xu, *Colloid Polym. Sci.* **2012**, *290*, 349.
- [47] S. Sennato, E. Chauveau, S. Casciardi, F. Bordi, D. Truzzolillo, *Polymers* **2021**, *13*, 1153.
- [48] S.-H. Jung, S. Schneider, F. Plamper, A. Pich, *Macromol. Chem.* **2020**, *53*, 1043.
- [49] X. Yang, H. Y. Lee, J.-C. Kim, *J. Appl. Polym. Sci.* **2011**, *120*, 2346.
- [50] S. Schmidt, T. Liu, S. Rütten, K.-H. Phan, M. Möller, W. Richtering, *Langmuir* **2011**, *27*, 9801.
- [51] M. Destribats, M. Wolfs, F. Pinaud, V. Lapeyre, E. Sellier, V. Schmitt, V. Ravaine, *Langmuir* **2013**, *29*, 12367.
- [52] M. Destribats, V. Lapeyre, E. Sellier, F. Leal-Calderon, V. Schmitt, V. Ravaine, *Langmuir* **2011**, *27*, 14096.
- [53] T. Yang, A. Cingolani, T. Casalini, A. Aribia, A. Klaue, H. Wu, S. Stavrakis, A. de Mello, M. Morbidelli, *Adv. Mater. Technol.* **2019**, *4*, 1900092.
- [54] T. Ngai, H. Auweter, S. H. Behrens, *Macromol. Chem.* **2006**, *39*, 8171.
- [55] T. Ngai, S. H. Behrens, H. Auweter, *Chem. Commun.* **2005**, 331.
- [56] W. D. Bancroft, *J. Phys. Chem.* **1912**, *16*, 177.
- [57] P. Finkle, H. D. Draper, J. H. Hildebrand, *J. Am. Chem. Soc.* **1923**, *45*, 2780.
- [58] C. Priest, M. D. Reid, C. P. Whitby, *J. Colloid Interface Sci.* **2011**, *363*, 301.
- [59] A. Tuominen, T. Sundman, *Phytochem. Anal.* **2013**, *24*, 424.
- [60] C. Dupont, F. De Vuyst, A.-V. Salsac, *J. Fluid Mech.* **2023**, *955*, A2.
- [61] X. Q. Hu, B. Sévénié, A. V. Salsac, E. Leclerc, D. Barthès-Biesel, *Phys. Rev. E* **2013**, *87*, 063008.
- [62] X. Q. Hu, A. V. Salsac, D. Barthès-Biesel, *J. Fluid Mech.* **2012**, *705*, 176.
- [63] I. Erel-Unal, S. A. Sukhishvili, *Macromol. Chem.* **2008**, *41*, 8737.
- [64] V. Kozlovskaya, E. Kharlampieva, I. Drachuk, D. Cheng, V. V. Tsukruk, *Soft Matter* **2010**, *6*, 3596.
- [65] T. Cubaud, T. G. Mason, *Phys. Fluids* **2008**, *20*, 053302.
- [66] Z. Nie, M. Seo, S. Xu, P. C. Lewis, M. Mok, E. Kumacheva, G. M. Whitesides, P. Garstecki, H. A. Stone, *Microfluid. Nanofluid.* **2008**, *5*, 585.
- [67] W. Lee, L. M. Walker, S. L. Anna, *Phys. Fluids* **2009**, *21*, 032103.
- [68] A. J. D. Krüger, O. Bakirman, L. P. B. Guerzoni, A. Jans, D. B. Gehlen, D. Rommel, T. Haraszti, A. J. C. Kuehne, L. De Laporte, *Adv. Mater.* **2019**, *31*, 1903668.
- [69] A. Nakaishi, S. Minami, S. Oura, T. Watanabe, D. Suzuki, K. Urayama, *Macromol. Chem.* **2018**, *51*, 9901.
- [70] Q. Feng, D. Li, Q. Li, X. Cao, H. Dong, *Bioact. Mater.* **2022**, *9*, 105.
- [71] J. D. Tice, A. D. Lyon, R. F. Ismagilov, *Anal. Chim. Acta* **2004**, *507*, 73.
- [72] W. Zeng, Z. Tong, X. Shan, H. Fu, T. Yang, *Chem. Eng. Sci.* **2021**, *243*, 116799.
- [73] D. B. Trushina, T. V. Bukreeva, T. N. Borodina, D. D. Belova, S. Belyakov, M. N. Antipina, *Colloids Surf., B* **2018**, *170*, 312.
- [74] L. C. Dong, A. S. Hoffman, Y. Qi, *J. Biomater. Sci., Polym. Ed.* **1994**, *5*, 473.
- [75] M. Behra, S. Schmidt, J. Hartmann, D. V. Volodkin, L. Hartmann, *Macromol. Rapid Commun.* **2012**, *33*, 1049.
- [76] A. S. Vikulina, N. A. Feoktistova, N. G. Balabushevich, R. von Klitzing, D. Volodkin, *ACS Appl. Mater. Interfaces* **2020**, *12*, 57401.
- [77] M. Hu, N. Reichholf, Y. Xia, L. Alvarez, X. Cao, S. Ma, A. J. deMello, L. Isa, *Mater. Horiz.* **2022**, *9*, 1641.
- [78] J. E. S. van der Hoeven, H. Gurunaryanan, M. Bransen, D. A. M. de Winter, P. E. de Jongh, A. van Blaaderen, *Adv. Funct. Mater.* **2022**, *32*, 2200148.
- [79] L. Zhang, K. Chen, H. Zhang, B. Pang, C. H. Choi, A. S. Mao, H. Liao, S. Utech, D. J. Mooney, H. Wang, D. A. Weitz, *Small* **2018**, *14*, 1702955.
- [80] P. Majumder, U. Baxa, S. T. R. Walsh, J. P. Schneider, *Angew. Chem., Int. Ed.* **2018**, *57*, 15040.
- [81] M. Godoy-Gallardo, C. Labay, V. D. Trikalitis, P. J. Kempen, J. B. Larsen, T. L. Andresen, L. Hosta-Rigau, *ACS Appl. Mater. Interfaces* **2017**, *9*, 15907.
- [82] S. Jiang, L. Caire da Silva, T. Ivanov, M. Mottola, K. Landfester, *Angew. Chem., Int. Ed.* **2022**, *61*, 202113784.
- [83] R. J. R. W. Peters, M. Marguet, S. Marais, M. W. Fraaije, van, J. C. M. Hest, S. Lecommandoux, *Angew. Chem., Int. Ed.* **2014**, *53*, 146.
- [84] L. Hosta-Rigau, M. J. York-Duran, Y. Zhang, K. N. Goldie, B. Städler, *ACS Appl. Mater. Interfaces* **2014**, *6*, 12771.